IJST, Transactions of Mechanical Engineering, Vol. 38, No. M1, pp 45-56
Printed in The Islamic Republic of Iran, 2014

NUMERICAL INVESTIGATION OF LAMINAR FLOW AND HEAT TRANSFER IN HEXAGONAL DUCTS UNDER ISOTHERMAL AND CONSTANT HEAT FLUX BOUNDARY CONDITIONS*

O. TURGUT

Dept. of Mechanical Engineering, Faculty of Engineering, Gazi University, 06570 Maltepe, Ankara, Turkey
Email: oturgut@gazi.edu.tr

Abstract– Three-dimensional laminar flow and heat transfer characteristics in smooth hexagonal ducts with equal sides have been numerically investigated in the Reynolds number range from 300 to 2000. The numerical solutions are obtained for both axially and peripherally constant wall temperature (*T*) and heat flux (*H*2) thermal boundary conditions for five different values of the duct angle (θ = 30, 45, 60, 75, and 90^o). Local Fanning friction factor and Nusselt number are obtained along the duct. Hydrodynamic and thermal entrance lengths have been determined. The accuracy of the results obtained in this study is verified by comparing the results with those available in the literature. Results show that duct geometry plays an important role on both flow and heat transfer characteristics. It is seen that the thermal entrance length for *H*2 boundary condition is greater than that for *T* boundary condition. Minimum hydrodynamic and thermal entrance lengths are obtained for $\theta = 60^o$, regular duct. New correlations, important for the design of thermal equipment, are presented for the hydrodynamic and thermal entrance lengths, friction factor, and Nusselt number for $30^o \le \theta \le 90^o$ and $300 \le Re \le 2000$.

Keywords– Laminar flow, heat transfer, internal flow, noncircular duct

1. INTRODUCTION

The flow distribution, pressure drop, and heat transfer characteristics in laminar flow through straight ducts of uniform cross section depend on a number of factors, especially cross sectional shape, inlet velocity and temperature profiles, and boundary condition [1]. The cross section of the duct can be both orthogonal (square or rectangular) and non orthogonal (triangular, trapezoidal, hexagonal).

Flow and heat transfer of the three-dimensional forced convection in hexagonal ducts are of importance for the design of thermal equipment. Hexagonal shapes are commonly used in compact heat exchangers which supply higher heat transfer rates [2]; these heat exchangers are employed in lamella type compact heat exchangers, which find wide usage in pulp and paper, alcohol, petrochemical, and other chemical industries [3]. Also, hexagonal cross section ducts are encountered in actuator-sensor structures which are commonly encountered in micro-scale fluidic devices [4]. The fluid flow in these ducts is three-dimensional, and owing to the small hydraulic diameter of the duct, the Reynolds number becomes so small that laminar flow generally prevails.

Comprehensive reviews of laminar flow and heat transfer in ducts of arbitrary cross section up to the nineties were presented by Shah and London [1] and Shah and Bhatti [5]. In addition, several fundamental studies of flow and heat transfer in hexagonal ducts have been presented in the past. Laminar fully developed flows through trapezoidal and hexagonal ducts were analyzed by Sadasivam et al. [3] using

*Received by the editors November 20, 2012; Accepted September 1, 2013.

finite difference method for constant axial wall heat flux with constant peripheral wall temperature (*H*1) and constant wall temperature peripherally as well as axially (*T*) thermal boundary conditions. Friction factor and Nusselt number for *T* and *H*1 boundary conditions are given for fully developed flow when $30^o \leq \theta \leq 75^o$. Viscous heating in liquids for fully developed flows in hexagonal micro-channels was numerically investigated by Morini [4]. It was found that viscous dissipation effect may be very important for liquid flows if the hydraulic diameter is less than 100 μm. Asako et al. [6] numerically studied three-dimensional developing laminar flow and heat transfer in the entrance region of a regular hexagonal duct for *T* and *H*1 boundary conditions for two Prandtl numbers (*Pr* = 0.7 and 8). The local Nusselt number along the duct and average Nusselt number up to the axial location *x* were obtained. Fully developed values of friction factor and Nusselt number were presented for *T* and *H*1 boundary conditions. Damean and Regtien [7] numerically investigated the velocity field of the fully developed laminar flow in a hexagonal duct used in actuator-sensor structures for side angles of $\theta = 60$ and 54.74^o. Analytical formulae were given to describe the velocity field. Pressure drop for fully developed laminar and turbulent flows in regular polygonal ducts was experimentally investigated by Nan [8]. An area equivalent round diameter was suggested to predict turbulent flow in a regular polygonal duct. Numerical study was conducted to obtain the temperature dependent viscosity effects on simultaneously developing laminar forced convection flow of a liquid in the entrance region of hexagonal duct with 54.74^o angle between sides under uniform wall temperature boundary condition by Nonino et al. [9]. Local friction factor and Nusselt number were given for both fluid heating and cooling. Results indicated that the effect of temperature dependent viscosity cannot be neglected in the entrance region of the laminar forced convection. Forced convection in a regular polygonal duct with a centered core was studied for *H*1 boundary condition using eigenfunction expansions and point match by Wang [10]. Friction factors and Nusselt numbers for fully developed flow are given for various core sizes.

It is seen from literature survey that some characteristics of laminar flow in hexagonal micro and macro-channels have been studied up to now.

Literature survey shows the lack of studies of three-dimensional laminar flow and heat transfer characteristics in the developing and fully developed flow regions of hexagonal duct for both axially and peripherally constant temperature (*T*) and heat flux (*H*2) boundary conditions. In this paper, numerical solutions have been carried out in smooth hexagonal ducts with equal sides for both axially and peripherally constant *T* and *H*2 boundary conditions using ANSYS FLUENT 12 software. Numerical study is implemented in the Reynolds number range of 300 to 2000 for five different side angles $\theta = 30$, 45, 60, 75, and 90^o. Correlations for hexagonal duct with equal sides are given for the hydrodynamic and thermal entry lengths under *T* and *H*2 thermal boundary conditions for $300 \leq Re \leq 2000$, $30 \leq \theta \leq 90^o$, and $Pr = 0.71$. Also, correlations for friction factor and heat transfer coefficients are given for *H*2 and *T* boundary conditions. The results of this study are expected to supply numerical data for three-dimensional laminar convective heat transfer in hexagonal ducts.

2. PROBLEM FORMULATION

The duct geometry, coordinate system and computational domain are shown in Fig. 1. Axis of the duct coincides with the *x*-axis of the coordinate system. The sides of the hexagonal duct are considered to be the same. In Fig. 1a, θ and β denote the left or right side angle and top or bottom corner angle, respectively; *a* and *b* are the half width and half height of the duct cross section, respectively, and *c* is the length of the side of the hexagonal duct. The flow is considered to be symmetric with respect to the *y*-*x* and *z*-*x* planes. Hence, only one quarter of the duct is considered for computational domain, which is shown in Fig. 1b.

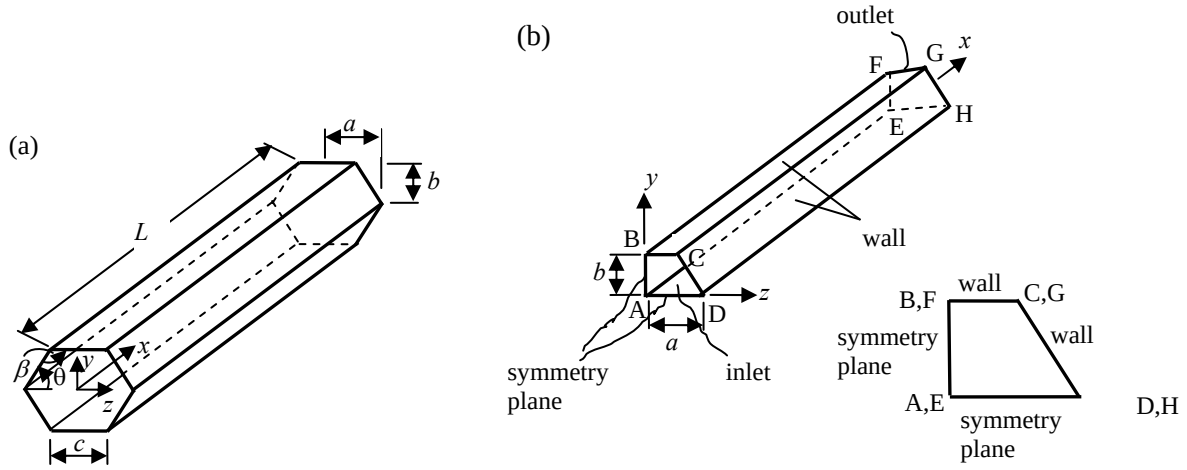

Fig. 1. (a) Duct geometry and coordinate system, (b) computational domain

The steady-state laminar flow of a constant-property viscous flow with negligible buoyancy effects and viscous dissipation is governed by the continuity, momentum, and energy equations as follow:

$$\nabla \cdot \boldsymbol{V} = 0 \tag{1}$$

$$\rho \frac{D\boldsymbol{V}}{Dt} = -\nabla p + \mu \nabla^2 \boldsymbol{V} \tag{2}$$

$$\rho c_{\mathrm{p}} \frac{DT}{Dt} = k \nabla^2 T \tag{3}$$

in which $\boldsymbol{V}$, T, ρ, p, μ, c_p, and k designate velocity vector, temperature, density, pressure, dynamic viscosity, specific heat, and thermal conductivity, respectively.

Governing equations are subjected to the following boundary conditions and shown in Fig. 1b:
At the inlet ($x = 0$, ABCD plane), fluid enters the duct with uniform velocity and temperature, i.e.,

$$u = u_{\mathrm{i}}, \quad v = 0, \quad w = 0, \quad T = T_{\mathrm{i}} \tag{4}$$

At the outlet ($x = L$, EFGH plane), it is considered that variations of all the variables in flow direction are negligible, i.e.,

$$\partial u/\partial x = 0, \quad \partial v/\partial x = 0, \quad \partial w/\partial x = 0, \quad \partial T/\partial x = 0 \tag{5}$$

On the symmetry plane at $z = 0$ (ABFE plane), symmetry conditions are applied, i.e.,

$$\partial u/\partial z = 0, \quad \partial v/\partial z = 0, \quad w = 0, \quad \partial T/\partial z = 0 \tag{6}$$

On the symmetry plane at $y = 0$ (AEHD plane), symmetry conditions are applied, i.e.,

$$\partial u/\partial y = 0, \quad v = 0, \quad \partial w/\partial y = 0, \quad \partial T/\partial y = 0 \tag{7}$$

On the duct surfaces (BFGC and CGHD surfaces), no slip velocity condition is applied. For temperature two different cases are considered: *i*) constant temperature, *ii*) constant heat flux. These can be expressed as:

$$u = 0, \quad v = 0, \quad w = 0, \quad T = T_{\mathrm{w}} \quad \text{or} \quad \partial T/\partial n = q'' / k \tag{8}$$

where n points out the direction of the outer normal to the boundary.

The Reynolds number Re is defined on the basis of inlet velocity and hydraulic diameter, i.e.,

$$Re = \rho D_h u_i/\mu \tag{9}$$

Here u_i is the uniform inlet velocity. D_h is the hydraulic diameter of the hexagonal duct and defined by $D_h = 4A_c /P$, where A_c is the cross sectional area and P is the wetted perimeter. For a hexagonal duct, hydraulic diameter is obtained as $D_h = (4c/3)\,(1 + \mathrm{Cos}\theta)\,\mathrm{Sin}\theta$.

The flow and heat transfer results are presented in terms of the dimensionless Fanning friction factor and Nusselt number. The local peripheral mean Fanning friction factor f_x and Nusselt number Nu_x for non-circular ducts are expressed, respectively, as

$$f_x = 2\tau_{w,x} /\rho u_i^2 \tag{10}$$

$$Nu_x = q''_{w,x} D_h / k\,(T_w(x) - T_b(x)) \tag{11}$$

In Eq. (10), $\tau_{w,x}$ is the peripherally averaged shear stress on the wall at any axial location x and determined as

$$\tau_{w,x} = \frac{1}{P}\int_{\Gamma} \mu\left(\frac{\partial u}{\partial n}\right) ds \tag{12}$$

in which P, Γ and s indicate the wetted perimeter of the duct at any axial location x, boundary, and circumferential direction, respectively. In Eq. (11), $q''_{w,x}$ is the peripherally averaged heat flux on the wall at any axial location x and given by

$$q''_{w,x} = \frac{1}{P}\int_{\Gamma} q''\, ds = \frac{1}{P}\int_{\Gamma}\left(-k\frac{\partial T}{\partial n}\right) ds \tag{13}$$

$T_w(x)$ and $T_b(x)$ in Eq. (11) are the wall and bulk temperatures, respectively, at any axial location x, and k is the thermal conductivity. The wall temperature $T_w(x)$ and bulk temperature $T_b(x)$ at any axial location x are expressed, respectively, as

$$T_w(x) = \frac{1}{P}\int_{\Gamma} T_w ds \tag{14}$$

$$T_b(x) = \frac{1}{A_c u_m}\int_{A_c} uTdA_c \tag{15}$$

where u_m is the mean velocity. Air is used as the fluid (Pr = 0.71). All fluid properties are taken at the inlet temperature.

a) Numerical solution procedure

Numerical solutions were carried out using commercial software ANSYS FLUENT 12.0. The computational scheme used by ANSYS FLUENT Inc. is based on the finite volume discretization method. Uniform hexahedral (structured) grids were created in the plane perpendicular to the main flow direction as well as uniform grid distribution in the main flow direction. Typical grid distributions in the cross section for various θ are shown in Fig. 2a. A typical grid distribution in some part of the computational domain is also seen in Fig. 2b for $\theta = 60^o$.

Computations were implemented for laminar flow. Steady pressure-based solver is employed with second order upwind scheme for convective terms in the mass, momentum, and energy equations. SIMPLE-algorithm is utilized for pressure-velocity coupling.

The grid independence study is performed by changing the cell size inside the computational domain for all ducts used in the present study until the variation in Nusselt number and Fanning friction factor are

less than 0.7% and 0.1%, respectively. In order to investigate the grid size effect, computations are performed under various grid sizes varying from 762 × 16 × 8 to 2381 × 60 × 30 in the *x*-, *y*-, and *z*-coordinate directions at *Re* = 2000 for *T* and *H*2 boundary conditions. Typical results obtained with different grid sizes in the fully developed flow are given in Table 1 for *Re* = 2000 for a regular hexagonal duct $\theta = 60^{o}$.

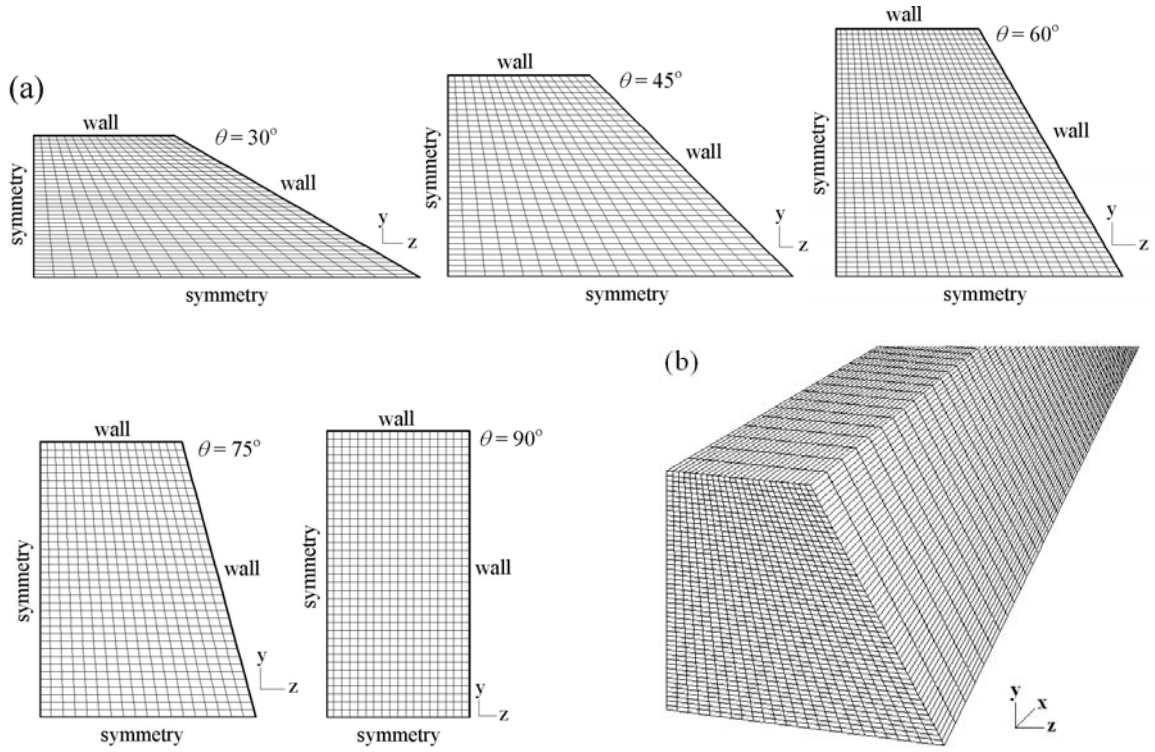

Fig. 2. Typical grid distribution (a) in the cross section for various θ and (b) in some parts of the computational domain for $\theta = 60^{o}$

Table 1. *Nu* and *fRe* values obtained with different grid systems at fully developed region for $\theta = 60^{o}$

Grid sizes	$(fRe)_{fd}$	Nu_{fd}	
		T	*H*2
762×16×8	14.997	3.352	4.244
950×20×10	15.030	3.349	4.161
1427×30×15	15.064	3.347	4.058
1713×36×18	15.073	3.346	4.026
1713×50×25	15.077	3.346	3.982
2381×50×25	15.083	3.345	3.982
2381×60×30	15.086	3.345	3.964
Shah and London [1]	15.054	3.340	3.862
Asako et al. [6]	15.065	3.353	

It is seen that a further refinement of grids from 1713 × 50 × 25 to 2381 × 60 × 30 produces no considerable change in the calculated fully developed values of Fanning friction factor and Nusselt number as shown in Table 1. The results of Shah and London [1] and Asako et al. [6] are also given in Table 1 for the purpose of comparison. As can be seen from Table 1, the present numerical results obtained with grid system 1713 × 50 × 25 are in close agreement with the literature results. Therefore, 1713 × 50 × 25 mesh size is assumed at $\theta = 60^{o}$ for both *T* and *H*2 boundary conditions. Similar grid size optimization is conducted for other θ values. No convergence problems are observed. To attain convergence, each equation is iterated until the residual falls below 1×10^{-6}.

3. RESULTS AND DISCUSSION

In this study, the laminar forced convective heat transfer and fluid friction in an air-cooled horizontal smooth duct having a hexagonal cross section with equal sides are numerically investigated. Numerical study has been carried out for *T* and *H*2 boundary conditions in the Reynolds number range of 300 to 2000 for five different side angles θ = 30, 45, 60, 75, and 90°. For θ = 90°, hexagonal duct reduces to a rectangular duct with the aspect ratio of 2. It should also be pointed out that hexagonal duct with θ = 60° is a regular hexagonal duct. For the ducts considered in the analysis, the length-to-hydraulic diameter ratio L/D_h is taken as 200. Hence, both developing and fully developed flow regions are analyzed simultaneously.

In order to assess the accuracy of the present computations, the computed fully developed values of the Nusselt number *Nu* and *fRe* are compared with the results of Shah [11], Farhanieh and Sunden [12], and Renksizbulut and Niazmand [13] in Table 2 for θ = 90°, rectangular duct. As can be seen from Table 2, the results of the present work are in good agreement with the corresponding literature values.

Table 2. Comparison of the fully developed values of *fRe* and *Nu* with results from literature for θ = 90°

		Present study	Shah [11]	F.&S. [12]	R.&N. [13]
$(fRe)_{fd}$		15.582	15.548	15.488	15.362
Nu_{fd}	*T*	3.430	3.391	3.393	3.403
	*H*2	3.231	3.020		

Typical dimensionless axial velocity profiles u/u_i at plane z = 0 (y-x symmetry plane, ABFE; see Fig. 1b) and at plane y = 0 (z-x symmetry plane, AEHD; see Fig. 1b) are plotted along the duct at various locations in Figs. 3a and 3b at *Re* = 1000 for θ = 60°. As seen in Figs. 3a and 3b, velocity profiles change up to the axial position x/D_h = 140. After axial position x/D_h = 140, velocity profiles do not change in the axial direction. In other words, flow is fully developed at x/D_h = 140. As expected and can be seen in Figs. 3a and 3b, axial velocity takes the zero and maximum values on the wall and centerline of the duct, respectively.

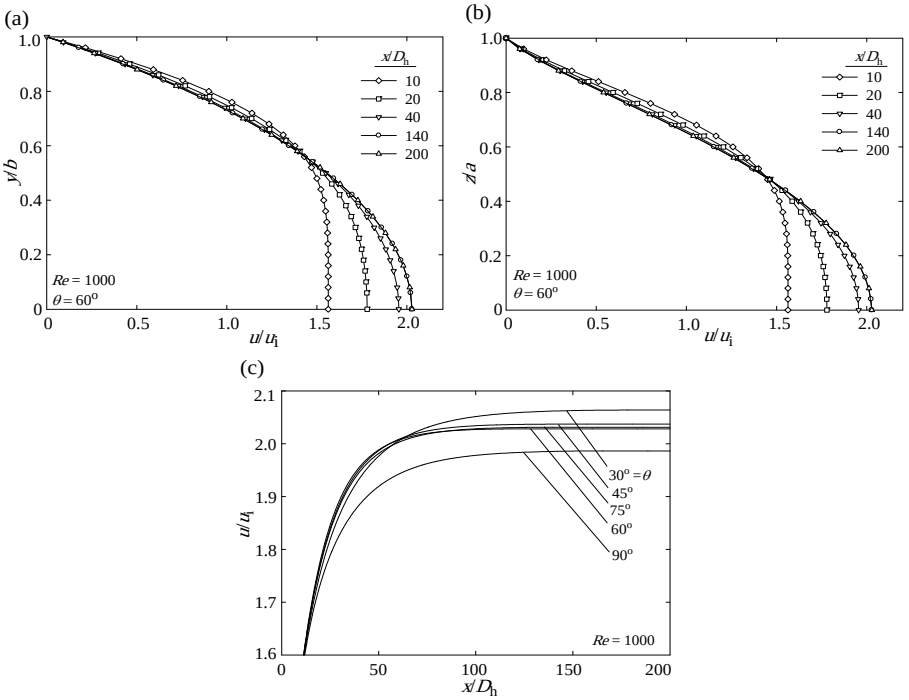

Fig. 3. Typical dimensionless axial velocity distribution on a plane at (a) z = 0 and (b) y = 0 along the duct (θ = 60°, *Re* = 1000); (c) typical dimensionless axial velocity variation on the centerline of the duct for different θ values (*Re* = 1000)

In Fig. 3c, dimensionless axial velocity u/u_i along the centerline of the duct (line AE, see Fig. 1b) is depicted for θ = 30, 45, 60, 75, and 90° at Re = 1000. It is seen that in both the hydrodynamic entrance region and in the fully developed region, the axial velocity changes with the duct angle θ.

In Fig. 4a the effect of the duct angle θ on fRe factor is given along the duct for Re = 1000. As seen in Fig. 4a, the duct angle θ affects the value of fRe factor in the entrance region as well as in the fully developed region. It is also seen that fRe increases with increasing θ in the fully developed region. The effect of Reynolds number on fRe factor is given in Fig. 4b along the duct for θ = 60°. As seen from Fig. 4b, fRe factor is maximum at the duct entrance, then decreases with increasing x and approaches a constant value in the fully developed region, i.e., becomes independent of x. At a given distance in the entrance region, fRe factor increases with increasing Reynolds number. It is seen that fRe factor depends on both the Reynolds number and axial position in the entrance region.

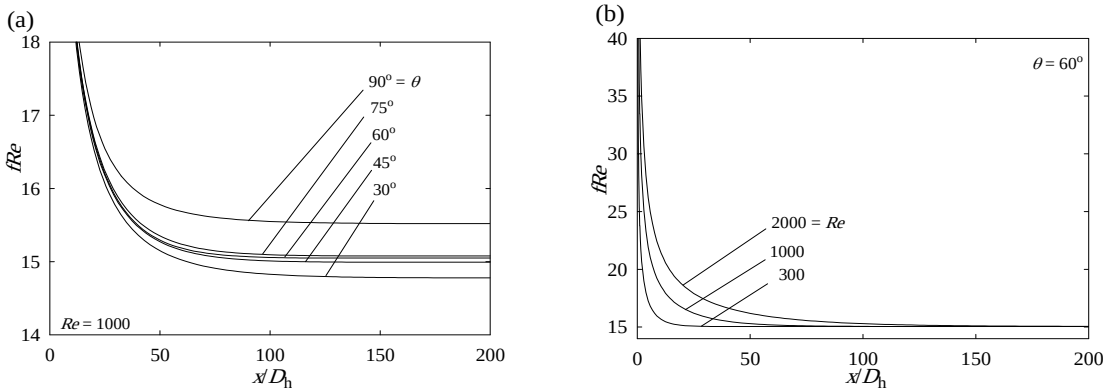

Fig. 4. (a) Local fRe along the duct for different θ values at Re=1000, (b) Local fRe along the duct for different Re at θ = 60°

Typical temperature contours on the cross section at x/D_h = 10, which is in the entrance region, are presented in Fig. 5 for Re = 1000 and five duct angles θ. It is seen that duct angle θ affects the temperature field.

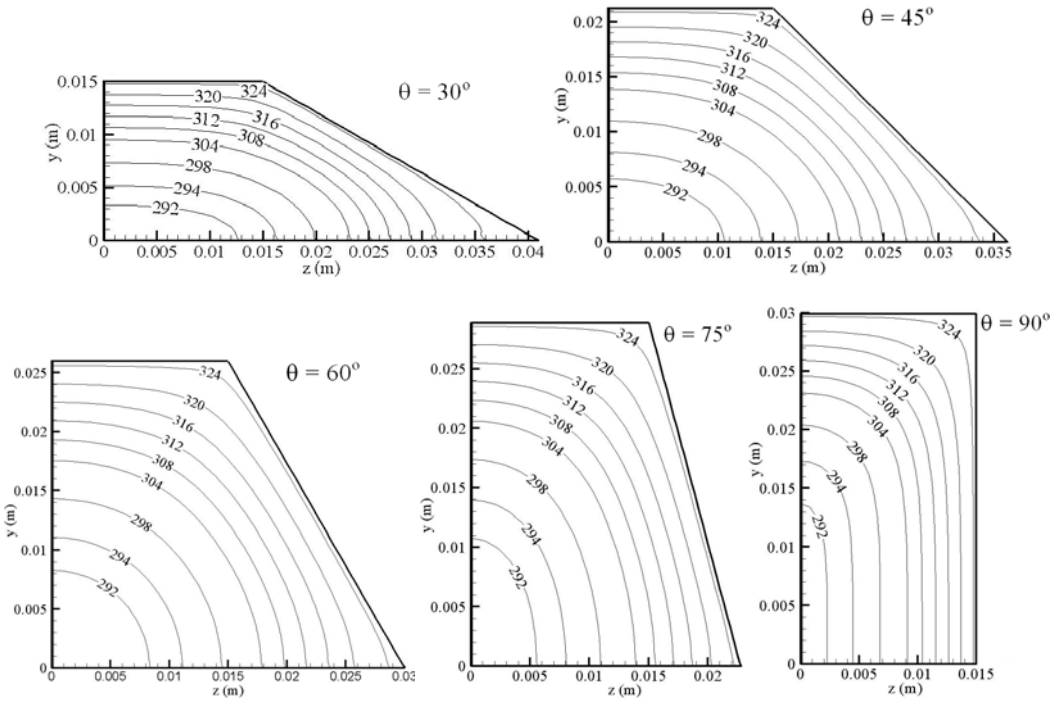

Fig. 5. Typical temperature contours for different θ values for constant temperature boundary condition (Re = 1000, x/D_h = 10)

To be able to see the effects of duct angle θ, thermal boundary condition, and Reynolds number on the local Nusselt number along the duct, local Nusselt number is plotted in Figs. 6a and 6b. Figure 6a shows the local Nusselt number along the duct at five different θ for both T and $H2$ boundary conditions. In Fig. 6b, local Nusselt number for T and $H2$ boundary conditions is plotted along the hexagonal duct with $\theta = 60^o$ for three different Reynolds numbers. As can be seen from Figs. 6a and 6b, local Nusselt number begins with a maximum value at the beginning of the duct, then it decreases with increasing x in the entrance region and approaches the constant value in the fully developed region. As will be seen from Fig. 6a, Nu_x approaches asymptotic value at about x/D_h=140 except for $\theta = 30^o$ for $H2$ boundary condition, for which it approaches fully developed condition later. This can be explained as a change in temperature distribution for $H2$ boundary condition at $\theta = 30^o$ (lowest duct angle) causes postponing of fully developed conditions, because temperature of the wall is not uniform peripherally and axially for $H2$ boundary condition. As can also be seen in Fig. 6, Nusselt number depends on the Reynolds number, thermal boundary condition, and the duct angle θ in the entrance region. However, in the fully developed region Nusselt number only depends on the thermal boundary condition and the duct angle θ. The values of Nu in the entrance region are much larger than the values in the fully developed region, as expected. This result indicates the significance of the entrance region in determining the heat transfer characteristics of short channels found in many modern miniaturized devices.

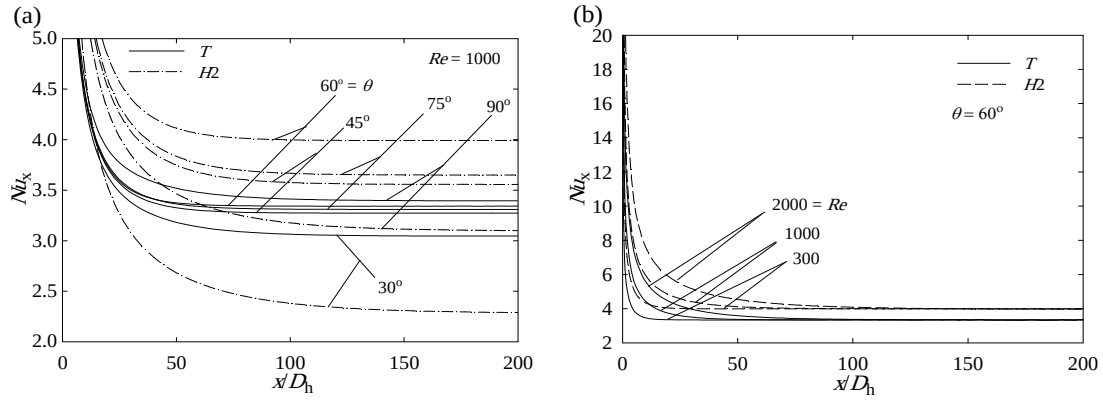

Fig. 6. (a) Local Nusselt number along the duct for different θ values at Re=1000, (b) Local Nusselt number along the duct for different Re

Fully developed values of fRe and Nu are given in Table 3 for five different θ values. As seen, fRe value increases with increasing θ. The change in fRe value from $\theta = 30$-90^o is about 4.7%. Hence, we may conclude that duct angle θ has no significant effect on fRe. It is also seen that Nusselt number for both thermal boundary conditions changes with the duct angle θ. However, effect of θ on Nusselt number with T and $H2$ boundary conditions is quite different. For T boundary condition, the change in the duct angle θ from 30 to 60^o increases Nusselt number. However, as θ increases further from 60 to 75^o, Nusselt number decreases. This can be attributed to the decreasing β as θ increases. Note that as θ increases from 60 to 75^o, top or bottom corner angle β decreases from 120 to 105^o. Nusselt number takes the maximum value at $\theta = 90^o$ (rectangular duct). For $H2$ boundary condition, Nusselt number increases with increasing θ from 30 to 60^o, and takes the maximum value at $\theta = 60^o$, then decreases with further increase in θ from 60 to 90^o. As seen in Table 3, Nusselt number in hexagonal duct with equal sides takes its maximum value for regular hexagonal duct $\theta = 60^o$, except $\theta = 90^o$ (rectangular duct). The results of Sadasivam et al. [3] for T boundary condition are also listed in Table 3 for comparison purpose. It is seen that the present results are in good agreement with those of Sadasivam et al. [3]. In Table 3, it is also seen that Nusselt number for $H2$ is less than the Nusselt number for T boundary condition for $\theta = 30^o$. That is, Nusselt number for $H2$ boundary condition is lower than the Nusselt number for T boundary condition for the duct geometries having strong corner effects. This result confirms the statement of Shah and London [1]. However, Nusselt

number for *H*2 is greater than the Nusselt number for *T* boundary condition for θ = 45-75^o. In addition, Nusselt number for *H*2 is less than the Nusselt number for *T* boundary condition for θ = 90^o; the result also agrees with the result of Shah [11] (see Table 2). Nusselt number results obtained in the present study for *H*2 boundary condition given in Table 3 for θ = 30, 45 and 75^o are the new results for literature. That is, θ except for 60 and 90^o has not been studied up to now for *H*2 thermal boundary condition. The ratio of *Nu* for *H*2 to the *Nu* for *T* boundary condition varies with θ from 0.79 to 1.19. This ratio for θ = 30^o is 0.79, for θ = 45^o is 1.10, for θ = 60^o is 1.19, for θ = 75^o is 1.11, and for θ = 90^o is 0.94. These results show the dependence of heat transfer and friction characteristics on the duct angle and wall condition. Figure 7 shows the temperature difference between wall and fluid bulk temperatures along the duct for *H*2 and *T* boundary conditions at θ = 30^o and 60^o. As can be seen in Fig. 7, temperature difference between wall and fluid bulk temperatures is higher for θ = 30^o than for θ = 60^o at *H*2 boundary condition in the fully developed region while it remains almost the same at *T* boundary condition. Thus, high temperature difference between wall and fluid bulk temperatures results in low heat transfer coefficient.

Table 3. Fully developed values of *fRe* and *Nu* for different θ

θ	$(fRe)_{fd}$		Nu_{fd}		
			T		*H*2
	Present study	Sadasivam et al. [3]	Present study	Sadasivam et al. [3]	Present study
30	14.880	14.757	3.085	3.144	2.427
45	15.041	14.859	3.280	3.376	3.599
60	15.077	14.974	3.346	3.431	3.982
75	15.126	14.967	3.318	3.433	3.690
90	15.582		3.430		3.231

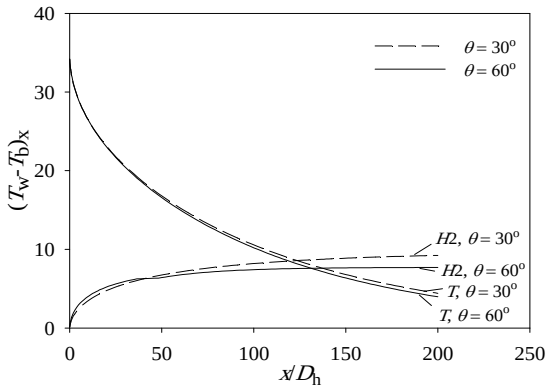

Fig. 7. Variation of $(T_w-T_b)_x$ along the duct

Hydrodynamic entrance length L_{hd} is defined as the axial location where maximum velocity attains 99% of its fully developed value. Based on this definition, the hydrodynamic entrance length is determined, and the values of L_{hd}/D_h are plotted in Fig. 8a as a function of *Re* for different θ values. It is seen that hydrodynamic entrance length depends on Reynolds number and the duct angle θ. Thermal entrance length L_{th} is the duct length required to achieve a value of the local Nu_x equal to 1.05*Nu* for fully developed flow when the entering fluid temperature profile is uniform [1]. Using this definition, thermal entrance length is obtained, and L_{th}/D_h is presented in Fig. 8b for *T* and *H*2 boundary conditions as a function of Reynolds number. As seen in Fig. 8b, thermal entrance length depends on Reynolds number, the duct angle θ, and the thermal boundary condition. The values of L_{hd}/D_hRe and L_{th}/D_hRe for developing flow are listed in Table 4 for five different θ values.

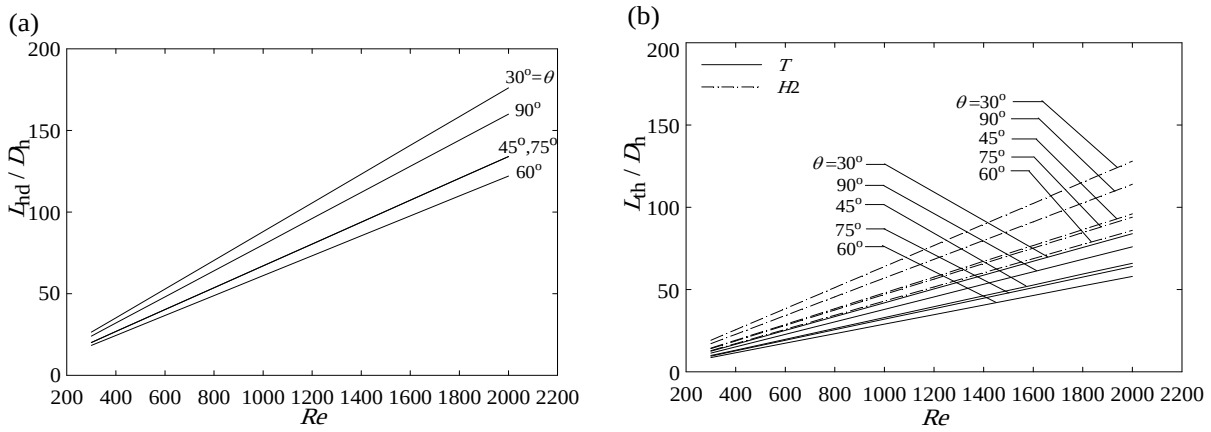

Fig. 8. Variation of (a) L_{hd}/D_h and (b) L_{th}/D_h versus Re for different duct angles

Table 4. Hydrodynamic and thermal entrance lengths for different θ

θ	$L_{hd}/(D_hRe)$		$L_{th}/(D_hRe)$	
	Present study	R.&N. [13]	T	$H2$
30	0.090		0.042	0.064
45	0.067		0.033	0.048
60	0.062		0.029	0.043
75	0.067		0.032	0.047
90	0.082	0.085	0.038	0.057

Present data given in Table 4 show that the hydrodynamic and thermal entrance length decreases with increasing θ from 30 to 60°, and takes its minimum value at θ = 60° (regular hexagonal duct), and then entrance length begins to increase with increasing θ. The thermal entrance length for $H2$ boundary condition is greater than that for T boundary condition. In other words, the thermal entrance length depends on the thermal boundary condition. The result of Renksizbulut and Niazmand [13] is also given in Table 4 for θ = 90° for comparison purpose. It is seen that the hydrodynamic entrance length obtained in the present work is in good agreement with that of Renksizbulut and Niazmand [13]; hydrodynamic entrance length was obtained using the maximum velocity value by Renksizbulut and Niazmand [13].

Results for friction factor and Nusselt number in the fully developed flow and hydrodynamic and thermal entrance lengths are correlated in the following form

$$fRe,\ Nu,\ L_{hd}/D_hRe, \text{ or } L_{th}/D_hRe = a_0 + a_1(\theta/\theta_o) + a_2(\theta/\theta_o)^2 + a_3(\theta/\theta_o)^3 + a_4(\theta/\theta_o)^4 \quad (16)$$

As can be seen in Eq. (16), duct angle θ is nondimensionalized by θ_o. Due to the fact that this study is carried out up to 90°, θ_o is taken as value 90°. The values of constants a_0 to a_4 are given in Table 5. Equation (16) represents the numerical values of L_{hd}/D_hRe, L_{th}/D_hRe for T boundary condition, L_{th}/D_hRe for $H2$ boundary condition, fRe, Nu for T boundary condition, and Nu for $H2$ boundary condition within ±0.1%, ±0.1%, ±0.1%, ±0.1%, ±0.2%, and ±0.1%, respectively, for $30 \le \theta \le 90°$, $300 \le Re \le 2000$, and Pr = 0.71.

Table 5. Values of constants a_0-a_4 in Eq. (16)

		a_0	a_1	a_2	a_3	a_4
L_{hd}/D_hRe		0.262	-0.924	1.608	-1.296	0.432
L_{th}/D_hRe	T	0.037	0.154	-0.657	0.828	-0.324
	$H2$	0.132	-0.275	0.200	0.054	-0.054
fRe		14.91	-3.427	17.56	-27.29	13.82
Nu	T	3.163	-3.646	16.98	-23.81	10.75
	$H2$	-0.770	6.662	21.60	-45.54	21.28

4. CONCLUSION

Three-dimensional laminar flow and heat transfer characteristics in the developing and fully developed flow regions of horizontal smooth hexagonal duct are numerically investigated under isothermal *T* and constant heat flux *H*2 boundary conditions for $300 \le Re \le 2000$, $30 \le \theta \le 90^o$, and $Pr = 0.71$. It is seen that duct angle θ and the type of thermal boundary condition affect the Nusselt number, friction factor and hydrodynamic and thermal entry lengths. It is also seen that the thermal entrance length for *H*2 boundary condition is higher than that of the *T* boundary condition. Minimum hydrodynamic and thermal entrance lengths are obtained for regular hexagonal duct $\theta = 60^o$. Correlations have been given for the hydrodynamic and thermal entrance lengths for $30^o \le \theta \le 90^o$ and $300 \le Re \le 2000$. In addition, new correlations have been given for the prediction of fully developed Nusselt number and friction factor values for *T* and *H*2 thermal boundary conditions for a wider range of duct angle θ.

Acknowledgements: The present work is financially supported by the Unit of Scientific Research Projects of Gazi University under the project BAP 06/2008-38.

NOMENCLATURE

a	half width of the duct cross section (m)
A_c	area of the cross section (m^2)
a_0-a_4	constant coefficients in Eq. (16) (-)
b	half height of the duct cross section (m)
c	edge length of the duct (m)
c_p	specific heat ($Jkg^{-1}K^{-1}$)
D_h	hydraulic diameter (m)
f_x	Local Fanning friction factor (-)
*H*1	constant axial wall heat flux with constant peripheral wall temperature boundary condition (-)
*H*2	axially and peripherally constant wall heat flux boundary condition (-)
k	thermal conductivity ($Wm^{-1}K^{-1}$)
L	length (m)
Nu_x	Local Nusselt number (-)
p	pressure (Pa)
P	perimeter of the cross section (m)
Pr	Prandtl number (-)
q''	heat flux (Wm^{-2})
Re	Reynolds number (-)
s	circumferential direction (m)
t	time (s)
T	isothermal boundary condition (-)
T	temperature (K)
u, v, w	velocity components (ms^{-1})
$\boldsymbol{V}$	velocity vector (ms^{-1})
x, y, z	coordinates (m)

Greek symbols

Γ	boundary (-)
β	top/bottom corner angle (deg)
μ	dynamic viscosity ($kgm^{-1}s^{-1}$)
θ	left/right side angle (deg)
ρ	density (kgm^{-3})
τ_w	shear stress (Pa)

Subscripts

b	bulk
hd	hydrodynamic entrance
i	inlet
m	mean
th	thermal entrance
w	wall

REFERENCES

1. Shah, R. K. & London, A. L. (1978). Laminar flow forced convection in ducts. in: Irvine, T. F. & Harnett, J. P. *Adv. Heat Transfer* (suppl. 1), Academic Press, New York, USA, pp. 5-60, p. 394.
2. Sohankar, A. (2010). Heat transfer and fluid flow through a ribbed passage in staggered arrangement. *Iranian Journal of Science & Technology: Transaction B: Engineering*, Vol. 34, pp. 471-485.
3. Sadasivam, R., Manglik, R. M. & Jog, M. A. (1999). Fully developed forced convection through trapezoidal and hexagonal ducts. *Int. J. Heat Mass Transfer*, Vol. 42, pp. 4321-4331.
4. Morini, G. L. (2005). Viscous heating in liquid flows in micro-channels. *Int. J. Heat Mass Transfer*, Vol. 48, pp. 3637-3647.

5. Shah, R. K. & Bhatti, M. S. (1987). Laminar convective heat transfer in ducts. in: Kakaç, S., Shah, R. K. & Aung, W., *Handbook of Single-Phase Convective Heat Transfer*, Wiley, New York, USA, Chapter 3.
6. Asako, Y., Nakamura, H. & Faghri, M. (1988). Developing laminar flow and heat transfer in the entrance region of regular polygonal ducts. *Int. J. Heat Mass Transfer*, Vol. 31, pp. 2590-2593.
7. Damean, N. & Regtien, P. P. L. (2001). Velocity field of the fully developed laminar flow in a hexagonal duct. *Sens. Actuators A*, Vol. 92, pp. 144-151.
8. Nan, S. (2001). Prediction of fully developed pressure drops in regular polygonal ducts. *ASME J. Fluid Mech.*, Vol. 123, pp. 439-442.
9. Nonino, C., Del Giudice, S. & Savino, S. (2006). Temperature dependent viscosiy effects on laminar forced convection in the entrance region of straight ducts. *Int. J. Heat Mass Transfer*, Vol. 49, pp. 4469-4481.
10. Wang, C. Y. (2011). Forced convection in a polygonal duct with a circular core. *ASME J. Heat Transfer*, Vol. 133, pp. 1-4.
11. Shah, R. K. (1975). Laminar flow friction and forced convection heat transfer in ducts of arbitrary geometry. *Int. J. Heat Mass Transfer*, Vol. 18, pp. 849-862.
12. Farhanieh, B. & Sunden, B. (1991). Three-dimensional laminar flow and heat transfer in the entrance region of trapezoidal ducts. *Int. J. Numer. Methods Fluids*, Vol. 13, pp. 537-556.
13. Renksizbulut, M. & Niazmand, H. (2006). Laminar flow and heat transfer in the entrance region of trapezoidal channels with constant wall temperature. *ASME J. Heat Transfer*, Vol. 128, pp. 63-74.